ENVIRONMENTAL RESEARCH
LETTERS

PURPOSE-LED PUBLISHING™

LETTER • OPEN ACCESS

The impact of long-lived cycle mesoscale eddies on air–sea CO_2 flux in the South Atlantic: focus on the full life cycle of the eddy

To cite this article: Xiaoke Liu *et al* 2025 *Environ. Res. Lett.* **20** 034033

IOP Publishing Environ. Res. Lett. 20 (2025) 034033 https://doi.org/10.1088/1748-9326/adb59d

ENVIRONMENTAL RESEARCH
LETTERS

LETTER

The impact of long-lived cycle mesoscale eddies on air–sea CO_2 flux in the South Atlantic: focus on the full life cycle of the eddy

Xiaoke Liu, Huisheng Wu*, Yanguo Fan, Yunlong Ji, Wenliang Zhou, Lejie Wang and Long Cui

College of Oceanography and Spatial Information, China University of Petroleum, Qingdao, People's Republic of China
* Author to whom any correspondence should be addressed.

E-mail: wuhuisheng@upc.edu.cn

Keywords: air–sea CO_2 flux, mesoscale eddy, machine learning

OPEN ACCESS

RECEIVED
4 November 2024

REVISED
6 January 2025

ACCEPTED FOR PUBLICATION
13 February 2025

PUBLISHED
21 February 2025

Abstract

Mesoscale eddies are prevalent in the global oceans and are known to influence oceanic and atmospheric conditions. This study aims to assess how the impact of mesoscale eddies on air–sea CO_2 fluxes varies throughout their lifecycle. We compared six machine learning models, including light gradient boosting machine, support vector machine, and XGBoost models, to construct an FCO_2 evaluation model. Among these, the XGBoost model performed the best, with model validation yielding the coefficient of determination (R^2) value of 0.9046 and a root mean square error of 1.4165 mmol m^{-2} d^{-1}, successfully assessing the air–sea CO_2 fluxes in the South Atlantic. Analysing eddies with a lifespan exceeding 300 d during the period from 1995 to 2020, we identified two distinct peaks in the influence of eddies on air–sea CO_2 fluxes during their life cycle: the first peak occurs approximately between the second and fifth deciles of the life cycle, during which the eddies have a broader impact range but weaker influence; the second peak emerges between the seventh and ninth deciles, exhibiting a narrower impact range but significantly stronger influence. These findings provide crucial quantitative evidence for understanding the marine carbon sequestration mechanism and reveal the complexity and dynamic nature of mesoscale eddies' impact on air–sea CO_2 fluxes.

1. Introduction

As one of the most significant carbon reservoirs on Earth, the ocean constantly engages in a CO_2 exchange with the atmosphere through the air–sea interface [1]. According to a 2019 assessment by the Global Carbon Project, oceans absorb an average of 2.5 ± 0.6 PgC − 1 annually, playing a pivotal role in mitigating the effects of climate change [2]. With the rise of global carbon cycle research, scholars have gradually deepened their understanding of the exchange mechanisms between the atmosphere and the ocean, quantifying the process through which atmospheric CO_2 enters the ocean via both physical and biological pathways. The air–sea carbon dioxide flux (FCO_2) serves as a proxy for this CO_2 exchange process, directly influencing variations in atmospheric CO_2 concentration and thereby exerting significant impacts on global climate patterns and ocean acidification. In recent years, an increasing number of studies have suggested that mesoscale eddies may significantly influence variations in FCO_2 [3–6].

Mesoscale eddies, ubiquitous dynamic structures within the ocean, exhibit spatial scales spanning from tens to hundreds of kilometres and persist for durations ranging from weeks to years [7, 8]. They can rapidly alter the ocean's surface environment and regulate the air–sea exchange of CO_2 by impacting the partial pressure of CO_2 and the overlying atmospheric conditions. Mesoscale eddies induce anomalies in sea surface temperature (SST) and sea surface salinity (SSS) [9], which directly affect the solubility of CO_2 in seawater, thereby regulating the air–sea exchange of CO_2. The vertical transport driven by these eddies significantly impacts the transport and distribution of marine nutrients and dissolved organic carbon [10], which can, in turn, affect the productivity of surface phytoplankton [11, 12]. Surface chlorophyll (CHL) concentration, a direct indicator of the

photosynthetic biomass in the upper ocean layer [13], is closely linked to phytoplankton productivity and is significantly influenced by mesoscale eddies [14]. Additionally, through interactions between the ocean and the atmosphere, eddies can locally alter sea surface wind speeds, thereby enhancing gas exchange rates and influence FCO_2 [15]. Considering these factors, this study selects SST, SSS, wind speed, and CHL as key parameters and employs machine learning models to build FCO_2 assessment models.

Throughout the life cycle of an eddy, its energy generally progresses through stages of formation, growth, and decline [16]. Currently, there is scant research on the differential influence of eddies on FCO_2 at different stages of their life cycle, and it is still uncertain whether these variations align with changes in eddy energy. Understanding the patterns of influence that eddies have on FCO_2 throughout their life cycle is crucial for air–sea carbon exchange and the oceanic carbon cycle.

The aim of this study is to uncover the patterns of influence that individual eddy has on FCO_2 throughout their life cycle. According to statistics, the average monthly displacement of long-lived cycle eddies in the South Atlantic Ocean is approximately 106 km, with eddy radius of about 68 km. Monthly data, which are commonly employed in research, tend to spatially broaden the impact of eddies and weaken potential characteristics simultaneously, thereby hindering the investigation into the influence of different stages of an eddy's life cycle on FCO_2. Based on this, our study integrates SOCAT underway data, remote sensing data, and introduces machine learning to build an FCO_2 estimation model, enabling the acquisition of FCO_2 data with high spatiotemporal resolution. Through the analysis of typical eddy events, we aim to reveal the patterns of influence that eddies have on FCO_2 at different developmental stages.

2. Materials and methods

The region spanning from 20°S to 60°S latitude and 35°W to 10°E longitude has been selected for this study. Located in the Southern Atlantic Ocean, this region is a hotspot for global carbon sink research, attracting the attention of numerous scholars who have conducted studies on carbon sinks in this area [3, 17, 18]. The area is primarily situated in deep-sea environments, where the generation and dissipation of eddies are not constrained by topographic features.

2.1. Remote sensing data

In this study, we utilised SST and SSS data obtained from the Copernicus Marine Service (CMEMS) GLOBAL_MULTIYEAR_PHY_001_030 product. CHL data were acquired from the CMEMS global ocean colour product, specifically the OCEANCOLOUR_GLO_BGC_L4_MY_009_104 dataset. These datasets have a temporal resolution of days and a spatial resolution of 0.083°. Additionally, wind speed data were derived from the cross-calibrated Multi-platform (CCMP) product of the remote sensing system, which provides daily wind speed as well as monthly average wind speed at 10 meters above sea level, with a spatial resolution of $0.25° \times 0.25°$.

The eddy data used in this study came from META3.1exp, a mesoscale eddy trajectory atlas product of satellite altimetry AVISO. Based on the absolute dynamic terrain data of the ocean, this product employs the Py Eddy Tracker algorithm and contour overlap to identify and track eddies. It includes information on eddy position, time, velocity and effective radius, amplitude, and associated profile and trajectories.

2.2. SOCAT observational data

The measured FCO_2 data for this study were provided in the form of Carbon dioxide fugacity (fCO_2) by the Surface Ocean CO_2 Atlas (SOCAT, version 2021), which also included a series of concurrent observational data such as SST, equilibrium temperature, SSS, and sea surface pressure; Supplementary variables were derived from interpolated global datasets. The SOCAT database [19] is the largest and most widely used database for fCO_2.

For this study, SOCAT observation data were selected from cruises flagged A-D and World Ocean Circulation Experiment cruises flagged 2, covering a total of 430 733 observations within the study region from 1995 to 2020.

2.3. Flux calculation

FCO_2 (mmol m^{-2} d^{-1}) can be calculated from

$$FCO_2 = kK_0\left(pCO_{2_{sea}} - pCO_{2_{air}}\right). \quad (1)$$

Where k is the gas transfer velocity (cm h^{-1}), K_0 is the solubility of CO_2 gas in seawater (mol kg^{-1} atm^{-1}). By dividing the fCO_2 provided by the SOCAT database by 0.996, $pCO_{2_{sea}}$ is obtained [20, 21]. Use the following formula to calculate $pCO_{2_{air}}$ [22]:

$$pCO_{2air} = xCO_2 \times \left(SLP - pH_2O^{air}\right). \quad (2)$$

In equation (2), sea surface CO_2 molar fraction (xCO_2) and sea level pressure are all derived from SOCAT observation data, and the saturated vapour pressure of water (pH_2O^{air}) is calculated by the following formula [23]:

$$pH_2O^{air} = \frac{\exp\left(34.494 - \frac{4924.99}{t+237.1}\right)}{(t+105)^{1.57}} \ (t > 0°C) \quad (3)$$

$$pH_2O^{air} = \frac{\exp\left(43.494 - \frac{6545.8}{t+278}\right)}{(t+868)^2} \quad (t \le 0^\circ C). \quad (4)$$

In the calculation of formulas (3) and (4), in order to avoid the accuracy of data products affecting the calculation of FCO_2, the temperature data is selected from the route record data. This paper uses the following formula to calculate k [24]:

$$k = 0.251 U^2{}_{10} \left(\frac{Sc}{660}\right)^{-0.5}. \quad (5)$$

The K_0 is determined according to equation (6) [25]:

$$\ln K_0 = A_1 + A_2(100/T) + A_3 \ln(T/100) + S\left[B_1 + B_2(T/100) + B_3(T/100)^2\right] \quad (6)$$

$A_1 = -58.0931$, $A_2 = 90.5069$, $A_3 = 22.2940$, $B_1 = 0.027\,766$, $B_2 = -0.025\,888$, $B_3 = 0.005\,0578$. T is SST and S is SSS. SST and SSS data were obtained from SOCAT observation data. U_{10} is the monthly average wind speed at 10 m above sea level, and Sc is the Schmidt number of surface water at field temperature. For FCO_2, a positive value means that CO_2 is released into the atmosphere, and a negative value means that the ocean absorbs CO_2.

2.4. Machine learning model selection

Machine learning models possess superior capabilities in capturing geological variable characteristics and addressing nonlinear issues, enabling the extraction of valuable information from vast datasets, thereby enhancing the accuracy and efficiency of analysis. Numerous scholars have introduced machine learning models into studies on FCO_2, addressing issues of data scarcity and insufficient accuracy to a certain extent [4, 22, 26, 27]. Different machine learning models possess distinct algorithmic structures and learning mechanisms, and comparing multiple models can help identify the optimal one for this study. XGBoost is a gradient boosting algorithm that takes into account more gradient enhancement information from the training dataset, featuring high efficiency and flexibility [28–31], along with a capability to resist overfitting. The XGBoost model approximates the objective function by employing a second-order Taylor expansion of the loss function. LightGBM is also a fast, well-distributed, high-performance machine learning framework, but it employs a 'histogram' algorithm to accelerate training [32]. Furthermore, deep learning, through its multi-layer structure, automatically learns features suitable for handling complex data, while neural network algorithms effectively process nonlinear relationships and fit complex functions. Both of these approaches have been applied in multiple studies on FCO_2 reconstruction [33, 34].

Therefore, this study selects six machine learning methods for comparative analysis: LightGBM, support vector machines (SVM), XGBoost, backpropagation neural networks, deep learning, and convolutional neural networks (CNN), for comparative analysis to select the optimal model.

2.5. Model evaluation

This study utilised SOCAT observation data from 1995 to 2020, encompassing over 430 000 data points from the South Atlantic Ocean, to train a model for estimating FCO_2. The *in-situ* measurements were matched with remote sensing data based on temporal and spatial information. To ensure randomness in the data, the order was shuffled, as the original sequence of cruise-based observations exhibited high spatial clustering.

The data were divided into two sets: 85% for model training and 15% for validation. Six different machine learning approaches were employed to establish the nonlinear relationship between FCO_2 and factors such as SST, SSS, wind speed, and CHL concentration. Based on the training results, the optimal model was selected.

The model evaluation was based on three statistical measures: the coefficient of determination (R^2), root mean square error (RMSE), and mean absolute percentage error (MAPE) as follows:

$$R^2 = \left[\frac{1}{N}\sum_{i=1}^{N}\left(\frac{X_i - \overline{X}}{\sigma_X}\right)\left(\frac{Y_i - \overline{Y}}{\sigma_Y}\right)\right]^2 \quad (7)$$

$$\mathrm{RMSE} = \sqrt{\frac{\sum_{i=1}^{N}(X_i - Y_i)^2}{N}} \quad (8)$$

$$\mathrm{MAPE} = \frac{\sum_{i=1}^{N}\left|\frac{Y_i - X_i}{Y_i}\right|}{N} \times 100\% \quad (9)$$

where, X_i, Y_i and N are respectively the predicted value, measured value and sample number of the model. $\overline{X}$ and $\overline{Y}$ are the mean values of the predicted and measured values, respectively. σ_X and σ_Y are the standard deviations of X_i and Y_i, respectively. The model training results are as follows (see table 1). Based on the training results, the XGBoost model has the best effect. In this paper, the XGBoost model is selected as the evaluation model for FCO_2 construction.

The model inversion results were verified, and the *in-situ* data and FCO_2 values predicted by XGBoost model were plotted as scatter density plots. R^2, RMSE and MAPE were selected as evaluation indexes. The verification results are shown in figure 1.

Table 1. Results of model training.

Case	R^2	RMSE (mmol m^{-2} d^{-1})	MAPE
XGBoost	**0.8950**	**1.6048**	**171.7056**
LightGBM	0.8134	2.1541	2877.0142
Deep learning	0.8116	2.1664	2243.4773
BP neural network	0.7581	2.4523	2568.9396
SVM	0.6279	3.0447	2505.9663
CNN	0.6740	2.8524	3.1963

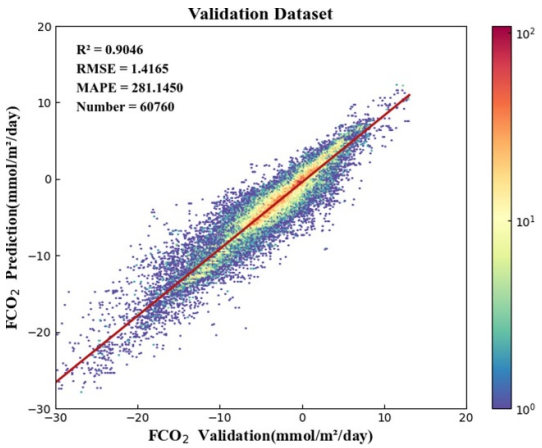

Figure 1. Verifies the set density scatter plot. The number of samples is 60 760, and the red line is the fitting line between the verification set and the prediction set.

3. Result

3.1. Variations in the influence of oceanic eddies on FCO_2 throughout their life cycle

By tracking the entire life cycle of the eddy, we have analysed the evolving patterns of its influence on FCO_2 from genesis to dissipation. Figure 2 illustrates the FCO_2 profile throughout the eddy's life cycle, with the eddy's effective area outlined by red dots. This eddy emerged in early January 2011 and dissipated by the end of October. Sampling monthly throughout its life cycle, we have observed the varying effects it had on FCO_2. In the initial and intermediate stages, represented by figures 2(a), (e), and (f), there were no noticeable differences between the eddy's effective area and its surrounding regions. However, in figures 2(b) and (c), a slight difference became apparent, with the eddy region exhibiting lower air–sea flux values compared to its surroundings. Figures 2(g) and (h) show distinct low-value points of FCO_2 within the effective regions of the eddies.

By comparing the FCO_2 values between scenarios with and without eddies present at the same location, we can further confirm that eddies have an impact on FCO_2. Additionally, taking into account the seasonal variations of FCO_2 and the potential delayed impacts that eddies could induce, we focused on a typical eddy that spent its entire life cycle in 2011. We preserved its location and retrieved FCO_2 data for the corresponding month in 2010 (see figure 3). Upon further observation, we found that when no eddy is present, no discernible pattern could be identified.

A random sample of 18 long-lived cycle eddies in South Atlantic was selected, and measures were taken to eliminate the confounding effects of seasonal variations on FCO_2 data. The FCO_2 data underwent a rigorous processing protocol. First, we computed the mean FCO_2 values within a region extending to three times the eddy's radius, centred precisely on the eddy. Next, we subtracted the mean FCO_2 values within a region defined by the eddy's radius itself from this value. A positive difference indicates that the FCO_2 concentration in the eddy region is relatively low, suggesting a stronger CO_2 sink. Conversely, a negative difference indicates the opposite effect. The study revealed that eddies had two peak impacts on FCO_2 throughout their entire life cycle (see figure 4). The first peak impact occurred between the second and fifth deciles of the life cycle, while the second peak was observed between the seventh and ninth deciles.

The analysis of the eddy's influence on FCO_2 during its peak periods, as shown in figures 5(a)–(d), revealed distinct characteristics based on the eddy's radius. During the first peak period (figures 5(a) and (b)), the eddy exhibited a large spatial extent, a relatively uniform effect, and a moderate impact. The effective influence boundary significantly exceeded the eddy's geometric radius, indicating a broader influence range compared to the second peak period. However, as the eddy progressed to the second peak period in figure 5(d), its impact on the FCO_2 became narrower in scope but significantly more potent.

3.2. Calculation of CO_2 sinks caused by eddy

To determine the CO_2 sink within the eddy region, we defined a circular area centred on the eddy's coordinates with a radius equal to the eddy's radius and calculated the CO_2 sink for this area. The studied eddy emerged in early 2011 and disappeared in late October 2011, with a life cycle exceeding 300 d. FCO_2 data were calculated for 20 periods, each 15 d long, and comparable data for 2010 were processed to obtain the mass of CO2 absorbed by the ocean in kilograms.

The calculations exhibited a strong dependency on the radius, causing the calculated results to fluctuate significantly due to this influence (see figure 6). By comparing the data from the same location at different times, it was observed that the peak difference in the amount of carbon absorbed in the region with an eddy occurs in the second peak region. In contrast, the first peak displayed a comparatively subdued effect. It was estimated that when the typical eddy existed, the eddy region absorbs about 66 061 tonnes over its entire life cycle, which is approximately four times more than during the non-eddy period.

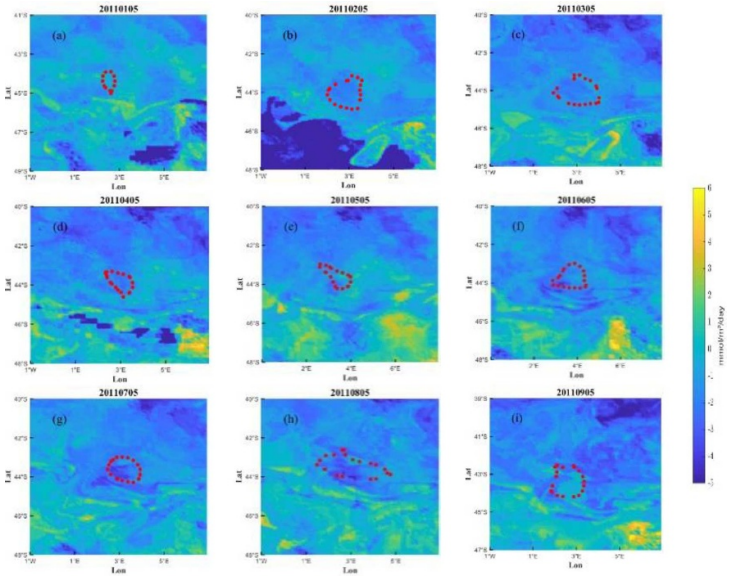

Figure 2. Full-cycle FCO_2 diagram of a typical eddy. The region surrounded by the red dot is the effective region of the eddy. Take figure (a) as an example, which is based on FCO_2 inversion data and eddy data on 5 January 2011, and can reflect the FCO_2 and eddy conditions of the day.

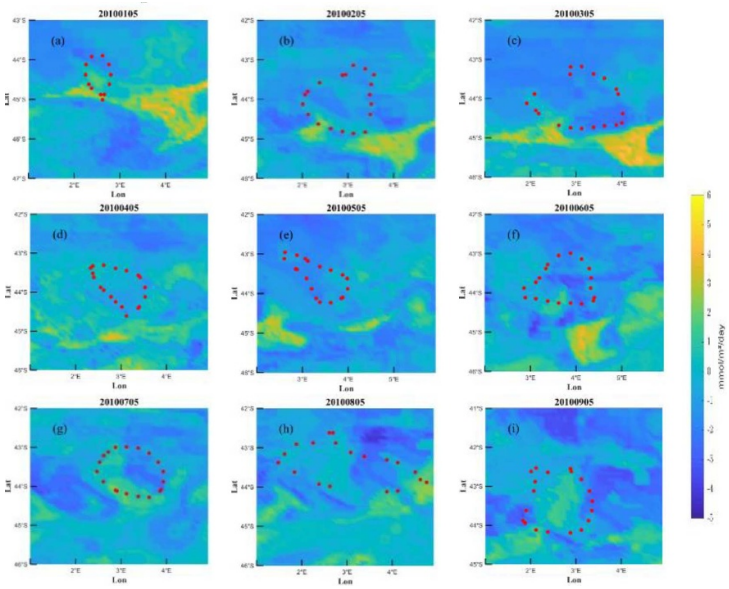

Figure 3. FCO_2 at the same position one year before a typical eddy. The area enclosed by red dots is the effective region of the eddy. As an example, similar to figure (a), this figure is based on the FCO_2 inversion data of 5 January 2010, and the eddy data of 5 January 2011, reflecting the FCO_2 conditions prior to the eddy's formation.

4. Discussion

From formation to dissipation, mesoscale eddies are in a state of constant development and movement, suggesting that their influence may exhibit corresponding fluctuations. To reveal the patterns of how eddies affect FCO_2 throughout their lifecycle, this paper has integrated field measurements with remote sensing data and employed machine learning to construct an FCO_2 assessment model. By monitoring the life paths of eddies, we assessed their influence on FCO_2 throughout their developmental stages.

Previous studies have generally categorized changes in eddy energy into three periods: the formation period, the peak period, and the dissipation period [16, 35]. The results of this study indicate a distinction between the variation in the impact of eddies on FCO_2 and the change in eddy energy, as shown in figure 2. In the early stages of eddy formation, its influence on FCO_2 continuously strengthens,

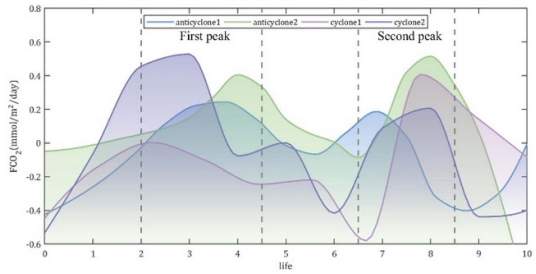

Figure 4. Variation curve of eddy influence with life cycle. The four long-lived cycle eddies are normalized, and the *X*-axis represents each stage of the life of the eddies. The *Y*-axis represents the difference between the eddy and the mean FCO_2 value of the surrounding environment, i.e. eliminating the effect of changes in the background field. The life cycle of the eddy is divided into five stages by four dotted lines. The second and fourth stages are the first and second peak stages of the eddy influence respectively.

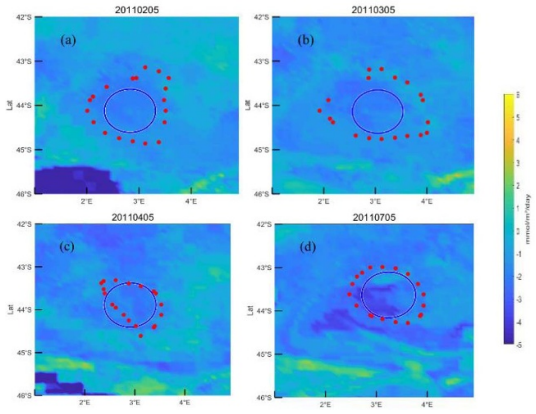

Figure 5. Radius characteristics of eddy influence during peak period. (a), (b) and (c) are in the first peak period, and (d) are in the second peak period. The area surrounded by red dots is the active area of the eddy, and the blue circle represents the radius circle of the eddy.

reaching the first peak value. Subsequently, its impact decays and then strengthens again, reaching a second peak before decaying until the eddy dissipates. This pattern is more evident in figure 4. The significant impact of eddies on FCO_2, characterized by two distinct peaks, is likely due to the multifaceted and complex interactions between marine physical processes and biological activities influenced by the eddies.

From the formation to the peak period of the eddy, the energy gradually increases, leading to the first peak value. At peak development, anticyclonic eddies drive downward vertical transport, depleting surface nutrients and diminishing biological activity. Simultaneously, the elevation of SST reduces the solubility of CO_2, and these combined effects lead to a reduction in the eddy's impact on FCO_2. During the maturity phase, as eddy wind speeds intensify, they augment the turbulence at the air–sea interface [36]. The modulation of the biological pump leads to a renewed increase in the concentration of surface nutrients, triggering the second peak in the eddy's influence on FCO_2. Cyclone eddies transport nutrients from the deep layers to the euphotic zone, promoting phytoplankton growth and enhancing the ocean's biological pump function [37]. Negative anomalies in SST and SSS increase CO_2 solubility, potentially leading to the first peak in the eddy's influence on FCO_2. The progression of cyclonic eddies can cause an abnormal increase in sea surface DIC, affecting sea surface carbon dioxide (pCO_2) [38]. Concurrently, a decrease in wind speed at the centre of cyclonic eddies is observed [36]. The combined effect of these factors may reduce the eddy's influence on FCO_2. Nutrients are continuously replenished to the surface through upwelling, and enhancing biological activity leads to the emergence of the second peak in FCO_2 influence. As mesoscale eddies enter their dissipation period, their energy wanes, and with it, the influence they exert on FCO_2 diminishes from a secondary peak to eventual dissipation. Throughout this decay, the eddy's radius, depth, amplitude, and kinetic energy undergo alterations, which in turn modulate its capacity to affect FCO_2.

Zhang *et al* [39] have revealed that mesoscale eddies, which are generated by various instabilities, form nuclearized coherent structures and approach the minimum-energy state through geostrophic adjustment. Structurally, eddies acquire energy under various instabilities, enhancing or maintaining their current state during their temporal evolution. This energy dynamics was reflected in our findings where, during the first peak period, the eddy's intensified state manifests as a broader influence on the sea surface, as indicated by the effective influence boundary significantly exceeding its geometric radius (figures 5(a) and (b)). As the eddy progresses, the balance between energy dissipation and absorption shifts, potentially leading to a contraction of its influence to maintain stability, which is evident in the second peak period where the influence range narrows and becomes more potent (figure 5(d)).

Considering the influence of eddies, as the eddy transitions from its formation to its peak phase, the broader influence range during the first peak leads to a widespread increase in primary productivity, resulting in a uniform distribution of the eddy's impact across its domain. However, as eddy currents concentrate the effects around its core, the distribution of FCO_2 values within the eddy's radius becomes uneven, especially under specific environmental conditions or variations in nutrient availability. This biological activity in certain areas may exceed that in others, leading to distinct dominant regions observed during the second peak period.

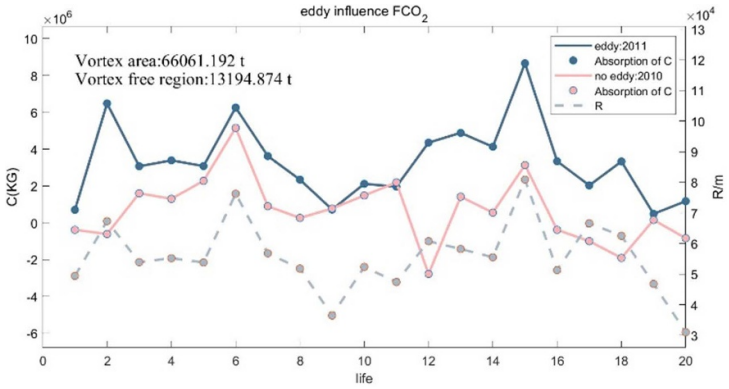

Figure 6. Calculation of typical eddy CO_2 sinks. The *X*-axis represents the stages of the life cycle, which are divided into 20 phases. The *Y*-axis is the *C* mass absorbed by the eddy region of each phase, in kg. The blue line is a typical eddy that arose in early January 2011 and died out in late October 2011, and the *C* mass absorbed by the eddy region in each period. The pink line represents the *C* mass absorbed by the same region in the same month the year before the eddy. The dashed grey line represents the radius of the eddy in m.

Long-lived eddies, characterized by their extended duration and broad impact, have a more significant effect on ocean FCO_2 compared to short-lived eddies. Therefore, this study specifically focuses on long-lived eddies to explore their impact patterns on FCO_2, and it remains to be explored whether the influence patterns of short-lived eddies align with those of their longer-lived counterparts. Furthermore, previous studies have confirmed the spatial heterogeneity of eddies' impact on FCO_2. For instance, Kim *et al* [6] found that the entire study area in the northern Philippines acted as a CO_2 source, while Orselli *et al* [3] indicated that mesoscale eddies enhance the CO_2 sink effect in the South Atlantic Ocean. The contrasting results from different oceanic regions demonstrate this point. However, our study solely focuses on the influence of long-lived eddy in the South Atlantic Ocean on FCO_2, and whether this pattern generalises to other regions remains to be verified.

This study estimated the CO_2 sink in the same region across different years, analysing the impact of eddies by comparing period with and without their presence. The calculations, which are inherently linked to the eddy radius, show that the CO_2 sink is consistently greater in the presence of an eddy (figure 6). The peak difference occurs in the late eddy period, specifically during the second peak interval shown in figure 4, while the valley of this difference appears in the middle of the eddy period, consistent with previous results. It was calculated that the typical eddy absorbed 66 062 tonnes of carbon during its lifetime. When compared to the cumulative FCO_2 estimations by Ford *et al* [4], our results are consistent after adjusting for eddy lifespan, thereby further validating the findings of this study. In the presence of the typical eddy, the influence region absorbed about four times more carbon than during the non-eddy period. According to statistics, within the study area alone, from 1995 to 2020, there were 390 cyclonic eddies and 522 anticyclonic eddies with a lifespan exceeding 300 d, averaging approximately 36 long-lived cycle eddies per year. As a common oceanic phenomenon, the impact of eddies on FCO_2 should not be overlooked.

5. Conclusion

This study proposes a novel method to evaluate the impact of long-lived cycle mesoscale eddies on FCO_2 in the South Atlantic Ocean. Based on remote sensing data, measured data and eddy data, an FCO_2 evaluation model was constructed using XGBoost to analyse the influence of eddies on FCO_2 throughout their life cycle. The results indicate that for long-lived cycle eddies, their influence on FCO_2 varies with eddy age. Compared to the surrounding environment, there are two peak periods: one spanning from the second to the fifth decile and another from the seventh to the ninth decile of the eddy's life cycle. Estimations of CO_2 sinks in the same location with and without eddies reveal that regions with eddies absorb more carbon. The typical eddy examined in this study absorbed approximately 66 061.192 tonnes of carbon in its effective area during its entire life cycle, which is approximately four times more than during non-eddy period. Therefore, long-lived cycle eddies significantly enhance the CO_2 sink in the South Atlantic Ocean. The findings of this study are significant for the refined assessment of oceanic carbon sinks. It is worth noting that this study focuses on long-lived cycle eddies in the South Atlantic Ocean and does not confirm whether the results apply to short-lived eddies or eddies in other oceanic regions.

Data availability statement

All data that support the findings of this study are included within the article (and any supplementary files).

Acknowledgment

This research was funded by the National Natural Science Foundation of China (Grant No. 42074028). We thank all contributors to the data products offered by Copernicus Maritime Services, which is the basis of this work. We thank remote sensing system for their cross-calibrated Multi-platform (CCMP) products, and CCMP Version-3.1 vector wind analyses are produced by Remote Sensing Systems. Data are available at www.remss.com. The surface ocean CO_2 Atlas (SOCAT) is an international effort, endorsed by the International Ocean Carbon Coordination Project (IOCCP), the Surface Ocean Lower Atmosphere Study (SOLAS), and the Integrated Marine Biogeochemistry and Ecosystem Research program (IMBER), to deliver a uniformly quality controlled surface ocean CO_2 database. The many researchers and funding agencies responsible for the collection of data and quality control are thanked for their contributions to SOCAT. The altimetric Mesoscale Eddy Trajectories Atlas (META3.1exp DT) was produced by SSALTO/DUACS and distributed by AVISO+ (Home (altimetry.fr)) with support from CNES, in collaboration with IMEDEA (https://doi.org/10.24400/527896/a01-2021.001 for the META3.1exp DT allsat version and https://doi.org/10.24400/527896/a01-2021.002 for the META3.1exp DT twosat version).

Data statement

Sea surface temperature (SST) and sea surface salinity (SSS) data are available from Copernicus Marine Services (CMEMS) Global Ocean Physics Reanalysis product (https://doi.org/10.48670/moi-00016). Chlorophyll data from Copernicus Marine Services (CMEMS) Global Ocean Colour products (10.48670/moi-00281). The AVISO+ Mesoscale Eddy Product META3.1exp can be downloaded from https://doi.org/10.24400/527896/a01-2021.001. The measured FCO_2 data for this study were provided in the form of fCO_2 by the Surface Ocean CO_2 Atlas (DOI: 10.25921/9wpn-th28). CCMP Version-3.1 vector wind analyses are produced by Remote Sensing Systems(https://doi.org/10.56236/RSS-uv6h30).

ORCID iD

Huisheng Wu https://orcid.org/0000-0001-8470-8476

References

[1] DeVries T 2022 The Ocean carbon cycle *Annu. Rev. Environ. Resour.* **47** 317–41
[2] Friedlingstein P *et al* 2020 Global carbon budget *Earth Syst. Sci. Data* **12** 3269–340
[3] Orselli I B M, Kerr R, Azevedo J L L D, Galdino F, Araujo M and Garcia C A E 2019 The sea-air CO2 net fluxes in the South Atlantic Ocean and the role played by Agulhas eddies *Prog. Oceanogr.* **170** 40–52
[4] Ford D J, Tilstone G H, Shutler J D, Kitidis V, Sheen K L, Dall'Olmo G and Orselli I B M 2023 Mesoscale eddies enhance the Air-Sea CO_2 sink in the South Atlantic Ocean *Geophys. Res. Lett.* **50** e2022GL102137
[5] Pezzi L P *et al* 2021 Oceanic eddy-induced modifications to air–sea heat and CO2 fluxes in the Brazil-Malvinas confluence *Sci. Rep.* **11** 10648
[6] Kim D, Lee S-E, Cho S, Kang D-J, Park G-H and Kang S K 2022 Mesoscale eddy effects on sea-air CO_2 fluxes in the northern Philippine Sea *Front. Mar. Sci.* **9** 970678
[7] Duo Z, Wang W and Wang H 2019 Oceanic mesoscale eddy detection method based on deep learning *Remote Sens.* **11** 1921
[8] Chelton D B, Schlax M G and Samelson R M 2011 Global observations of nonlinear mesoscale eddies *Prog. Oceanogr.* **91** 167–216
[9] Melnichenko O, Amores A, Maximenko N, Hacker P and Potemra J 2017 Signature of mesoscale eddies in satellite sea surface salinity data: SSS SIGNATURE OF MESOSCALE EDDIES *J. Geophys. Res. Oceans* **122** 1416–24
[10] Klein P and Lapeyre G 2009 The Oceanic vertical pump induced by mesoscale and submesoscale turbulence *Annu. Rev. Mar. Sci.* **1** 351–75
[11] Lin J, Cao W, Wang G and Hu S 2014 Satellite-observed variability of phytoplankton size classes associated with a cold eddy in the South China Sea *Mar. Pollut. Bull.* **83** 190–7
[12] Cornec M, Laxenaire R, Speich S and Claustre H 2021 Impact of mesoscale eddies on deep chlorophyll maxima *Geophys. Res. Lett.* **48** 15
[13] Tian F and Zhang R-H 2023 Decreasing surface chlorophyll in the tropical ocean as an indicator of anthropogenic greenhouse effect during 1998–2020 *Environ. Res. Lett.* **18** 084019
[14] He Q, Zhan H, Cai S and Li Z 2016 Eddy effects on surface chlorophyll in the northern South China Sea: mechanism investigation and temporal variability analysis *Deep-Sea Res. I* **112** 25–36
[15] Frenger I, Gruber N, Knutti R and Münnich M 2013 Imprint of Southern Ocean eddies on winds, clouds and rainfall *Nat. Geosci.* **6** 608–12
[16] Zhang Z, Xie L, Zheng Q, Li M, Li J and Li M 2022 Coherence of eddy kinetic energy variation during eddy life span to low-frequency ageostrophic energy *Remote Sens.* **14** 3793
[17] Wang Y, Li X, Song J, Li X, Zhong G and Zhang B 2021 Carbon sinks and variations of p CO_2 in the Southern Ocean from 1998 to 2018 based on a deep learning approach *IEEE J. Sel. Top. Appl. Earth Obs. Remote Sens.* **14** 3495–503
[18] Wang S and Moore J K 2012 Variability of primary production and air-sea CO_2 flux in the Southern Ocean *Glob. Biogeochem. Cycles* **26** 2010GB003981
[19] Bakker D C E *et al* 2016 A multi-decade record of high-quality fCO_2 data in version 3 of the surface Ocean CO_2 Atlas (SOCAT) *Earth Syst. Sci. Data* **8** 383–413
[20] Rödenbeck C, DeVries T, Hauck J, Le Quéré C and Keeling R F 2022 Data-based estimates of interannual sea–air CO_2 flux variations 1957–2020 and their relation to environmental drivers *Biogeosciences* **19** 2627–52
[21] Rödenbeck C, Keeling R F, Bakker D C E, Metzl N, Olsen A, Sabine C and Heimann M 2012 Sea-air CO_2 flux estimated from SOCAT surface-ocean CO_2 partial pressure data and

atmospheric CO_2 mixing ratio data *Ocean Sci. Discuss.* **9** 2273–326
[22] Yu S, Song Z, Bai Y, Guo X, He X, Zhai W, Zhao H and Dai M 2023 Satellite-estimated air-sea CO2 fluxes in the Bohai Sea, Yellow Sea, and East China Sea: patterns and variations during 2003–2019 *Sci. Total Environ.* **904** 166804
[23] Huang J 2018 A simple accurate formula for calculating saturation vapor pressure of Water and Ice *J. Appl. Meteorol. Climatol.* **57** 1265–72
[24] Wanninkhof R 2014 Relationship between wind speed and gas exchange over the ocean revisited *Limnol. Oceanogr. Methods* **12** 351–62
[25] Weiss R F 1974 Carbon dioxide in water and seawater: the solubility of a non-ideal gas *Mar. Chem.* **2** 203–15
[26] Couespel D, Tjiputra J, Johannsen K, Vaittinada Ayar P and Jensen B 2024 Machine learning reveals regime shifts in future ocean carbon dioxide fluxes inter-annual variability *Commun. Earth Environ.* **5** 99
[27] Zeng J, Iida Y, Matsunaga T and Shirai T 2022 Surface ocean CO_2 concentration and air-sea flux estimate by machine learning with modelled variable trends *Front. Mar. Sci.* **9** 989233
[28] Zhang Y *et al* 2022 Improving remote sensing estimation of Secchi disk depth for global lakes and reservoirs using machine learning methods *GIScience Remote Sens.* **59** 1367–83
[29] Carrión D, Arfer K B, Rush J, Dorman M, Rowland S T, Kioumourtzoglou M-A, Kloog I and Just A C 2021 A 1-km hourly air-temperature model for 13 northeastern U.S. states using remotely sensed and ground-based measurements *Environ. Res.* **200** 111477
[30] Qiu Y, Zhou J, Khandelwal M, Yang H, Yang P and Li C 2022 Performance evaluation of hybrid WOA-XGBoost, GWO-XGBoost and BO-XGBoost models to predict blast-induced ground vibration *Eng. Comput.* **38** 4145–62
[31] Xia Y *et al* 2022 Rapid assessments of light-duty gasoline vehicle emissions using on-road remote sensing and machine learning *Sci. Total Environ.* **815** 152771
[32] Dorogush A V, Ershov V and Gulin A 2018 CatBoost: gradient boosting with categorical features support
[33] Zhang S, Chen P, Hu Y, Zhang Z, Jamet C, Lu X, Dionisi D and Pan D 2023 Research ReportDiurnal global ocean surface pCO_2 and air–sea CO_2 flux reconstructed from spaceborne LiDAR data ed L Thompson *PNAS Nexus* **3** pgad432
[34] Wrobel-Niedzwiecka I, Kitowska M, Makuch P and Markuszewski P 2022 The distribution of pCO_2W and Air-Sea CO_2 fluxes using FFNN at the continental shelf areas of the Arctic Ocean *Remote Sens.* **14** 312
[35] Ren Q *et al* 2023 Three-dimensional structure of mesoscale eddies and their interaction with Kuroshio based on observations from a CPIES array *Front. Mar. Sci.* **10** 1109894
[36] Cabrera M 2022 The southwestern Atlantic Ocean mesoscale eddies: a review of their role in the air-sea interaction processes *J. Mar. Syst.* **235** 103785
[37] Zhao D 2021 Global chlorophyll distribution induced by mesoscale eddies *Remote Sens. Environ.* **254** 1
[38] Keppler L, Eddebbar Y A, Gille S T, Guisewhite N, Mazloff M R, Tamsitt V, Verdy A and Talley L D 2024 Effects of mesoscale eddies on Southern Ocean biogeochemistry *AGU Adv.* **5** e2024AV001355
[39] Zhang Z, Wang G, Wang H and Liu H 2024 Three-dimensional structure of oceanic mesoscale eddies *Ocean Land Atmos. Res.* **3** 0051